Available online at www.sciencedirect.com
ScienceDirect
Trans. Nonferrous Met. Soc. China 34(2024) 798−811
Transactions of Nonferrous Metals Society of China
www.tnmsc.cn

Effects of Zn and Gd contents and their ratios on microstructure and mechanical properties of as-cast and as-extruded Mg−8Li alloys

Yu-chuan HUANG[1,2,3], Quan-da ZHANG[1,2], Si-jie OUYANG[3], Fu-zhen SUN[1,2], Jia-wei SUN[3], Hui-yu LI[1,2], Guo-hua WU[3], Pei-jun CHEN[4], Wen-cai LIU[3]

1. State Key Laboratory of Advanced Forming Technology and Equipment, China Academy of Machinery Science and Technology Group Co., Ltd., Beijing 100083, China;
2. Beijing National Innovation Institute of Lightweight Ltd., Beijing 100083, China;
3. National Engineering Research Center of Light Alloy Net Forming and State Key Laboratory of Metal Matrix Composites, School of Materials Science and Engineering, Shanghai Jiao Tong University, Shanghai 200240, China;
4. Luoyang Shengya Magnesium Alloy Technology Co., Ltd., Luoyang 471921, China

Received 5 September 2022; accepted 14 February 2023

Abstract: The effects of contents of Zn and Gd elements and their mass ratios on microstructure and mechanical properties of as-cast and as-extruded Mg−8Li alloys were investigated. After extrusion, the precipitates are broken, and fine spherical particles with size about 100 nm are found to disperse in the β-Li. The bi-modal structure consisting of long-strip-like coarse-grain α-Mg and recrystallized fine-grain β-Li is formed. The strength and plasticity of the alloys are greatly improved after extrusion, and the YS and UTS increase with the increase of Zn and Gd contents. The Mg−8Li−8Zn−2Gd alloy exhibits an optimum comprehensive performance with the YS of 274 MPa, UTS of 283 MPa, and EL of 39.9%. The bi-modal structure strengthening consisting of the fine crystal strengthening of β-Li and texture strengthening of α-Mg, and the dispersion strengthening of precipitations are the main strengthening mechanisms.
Key words: Mg−Li alloy; extrusion deformation; bi-modal structure; dispersion strengthening

1 Introduction

The lightweight of metal structure materials is conducive to energy conservation and emission reduction, which has attracted more and more attention in recent years. Mg−Li alloys are the lightest metal-structural materials known at present, which have good ductility, and considerable specific strength and modulus [1,2]. However, the low absolute strength is one of the main factors limiting practical applications. Adding alloying elements and plastic deformation (extrusion, rolling, and forging) are effective methods to improve the comprehensive mechanical properties of Mg−Li alloys [3].

Zn element is an important strengthening alloying element in the Mg−Li-based alloys, which can not only enhance the strength of Mg−Li alloys but also has little bad effect on ductility [4,5]. However, Mg−Li−Zn alloys have an obvious over-aging softening phenomenon due to the transition of metastable phases ($MgLi_2Zn$ → MgLiZn) [6]. One approach to improve the thermal stability and strength of Mg−Li alloys is to add rare-earth elements (RE) due to the formation of thermally stable RE-containing phases and grain refinement [6]. In traditional Mg−Zn−RE alloys, the formation of complex Mg−Zn−RE ternary phases (Mg_3Zn_6RE and $Mg_3Zn_3RE_2$) can contribute to excellent mechanical properties [7−9]. Similarly, adding Zn and RE into Mg−Li alloys, including Y,

Corresponding author: Wen-cai LIU, Tel: +86-21-54742630, Fax: +86-21-34202794, E-mail: liuwc@sjtu.edu.cn
DOI: 10.1016/S1003-6326(23)66435-0

Gd, and Er, can also help to overcome the deficiency of poor strength [10]. Researchers in Refs. [11−14] have reported that the formation of the *W*-phase ($Mg_3Zn_3RE_2$) and *I*-phase (Mg_3Zn_6RE) is dependent on the Zn/RE ratio. XU et al [11] have found that *I*-phase and *W*-phase were both formed when Zn/RE mass ratios are 2.86 and 1.78, respectively. Previous studies [15] suggested that the Zn/RE mass ratios of the *I*-phase and *W*-phase were 4.38 and 1.10, respectively. In addition, ZHANG et al [10] indicate that the strength of the as-extruded Mg−Li−Zn−Gd alloys is determined by the volume fraction of the *I*-phase. Based on these findings, two further questions can be raised: (1) Can the contents of Zn and Gd influence the microstructure of Mg−Li−Zn−Gd alloys with the same Zn/RE ratio? (2) What is the main strengthening mechanism in the as-extruded Mg−Li−Zn−Gd alloys?

In this work, the Mg−8Li alloy with dual phase was selected as the base alloy, which combined the moderate strength of the α-Mg phase with good ductility of the β-Li phase. Based on the above findings, Zn/Gd mass ratio was chosen to be 2 and 4, aiming to get both *W*-phase and *I*-phases [11,15]. Mg−8Li−2Zn−1Gd and Mg−8Li−*x*(4Zn−1Gd) (*x*=1, 1.5, and 2 wt.%) alloys were designed. The target was to answer the above two questions by investigating the effects of the contents of Zn and Gd elements and their mass ratios on the microstructure and mechanical properties of the Mg−8Li alloys before and after hot extrusion. This study is of great significance for the development of high-strength and lightweight Mg−Li alloys.

2 Experimental

In this work, the designed Mg−Li−Zn−Gd alloys were prepared with commercially pure magnesium (99.99 wt.%), lithium (99.99 wt.%), zinc (99.99 wt.%) and Mg−30wt.%Gd master alloy. Raw materials with calculated mass were smelted in a vacuum induction furnace. Argon acting as the protected gas was pumped into the furnace chamber. After the raw materials were melted, the melt was stirred electromagnetically for 3 min and kept for 10 min. Then, it was poured into a metal mold preheated to 200 °C. The as-cast Mg−Li−Zn−Gd alloys with different Zn and Gd contents and their mass ratios were homogenized at 200 °C for 2 h and then extruded at 250 °C with the extrusion ratio of 25 [10].

The samples for microstructure analysis were made by standard metallographic preparation. After polishing and etching with 4 vol.% nitric acid alcohol solution, the metallographic observation was conducted by optical microscope (OM, Zeiss Axiovert 40). In addition, more detailed morphology was observed by scanning electron microscope (SEM, Phenom XL), which was outfitted with the energy dispersive spectrometer (EDS). The fracture surface was also observed by SEM. The samples for transmission electron microscope (TEM) observation were made by the combination of an ultra-precision dimpling grinder and iron beam thinner. TEM observation was carried out by the JEM−2100 facility at 200 kV. The chemical compositions of the investigated alloys were listed in Table 1, which were analyzed by inductively coupled plasma-atomic emission spectrometry (ICP-AES, Avio 500). The actual composition was relatively close to the nominal composition. The phase compositions of the Mg−Li−Zn−Gd alloys were identified by X-ray diffraction (XRD, Ultima IV) with the radiation resource of Cu K_α, at the step size of 0.03° and scanning rate of 5 (°)/min. The grain sizes were measured by quantitative graphic analysis software Image Pro-plus 6.0. At least 5 optical metallographic photos were counted for each sample, and the average value was calculated. The Vickers hardness (HV) of the alloys was measured at ambient temperature with a load of 49 N and a loading time of 15 s. Each sample was tested for at least 5 hardness values and the average hardness was calculated. Specimens for tensile tests were machined into a rectangle with a gauge size of 15 mm × 3 mm × 2 mm by the electric spark linear cutting machine. The tensile tests at room temperature

Table 1 Actual chemical compositions of Mg−Li−Zn−Gd alloys

Alloy No.	Nominal composition	Zn/Gd mass ratio	Chemical composition/wt.%			
			Li	Zn	Gd	Mg
I	Mg−8Li−2Zn−1Gd	2	7.68	1.62	1.04	Bal.
II	Mg−8Li−4Zn−1Gd	4	8.04	3.31	1.05	Bal.
III	Mg−8Li−6Zn−1.5Gd	4	8.00	5.14	1.64	Bal.
IV	Mg−8Li−8Zn−2Gd	4	7.97	6.68	2.18	Bal.

were conducted at the rate of 1.0 mm/s on the Zwick/Roell Z020 tensile test machine equipped with an extensometer. The mechanical properties of each sample were tested for more than 3 valid values, and the average value and its error bar were calculated.

3 Results

3.1 Microstructures of as-cast and as-extruded Mg−Li−Zn−Gd alloys

Figure 1 shows the microstructures of the as-cast Mg−Li−Zn−Gd alloys, in which a typical duplex structure is presented. The matrix consists of the white α-Mg phase (hexagonal close-packed structure) and the gray β-Li phase (body-centered cubic structure) [11,16−19]. With the increase of Zn and Gd contents, the number of α-Mg grains decreases, and the second phase changes from particle-like to net-like. With increasing the contents of Zn and Gd, the size of α-Mg grains decreases, as shown in Table 2. The optical microstructure of as-extruded alloys perpendicular to the extrusion direction is presented in Fig. 2. The α-Mg phase is severely deformed, and fine black particles are uniformly distributed in the matrix. Similarly, the optical microstructure of the as-extruded alloys parallel to the extrusion direction is shown in Fig. 3. The white α-Mg is stretched into long strips along the extrusion direction, and the gray β-Li changes from continuous structure to equiaxed grains with different sizes. The average size of β-Li with the Zn/Gd mass ratio of 4 (about 5 μm) is obviously less than that with the Zn/Gd mass ratio of 2 (about 20 μm). The recrystallized β-Li grains of Alloy Ⅳ are more uniform and finer, indicating that dynamic recrystallization occurred during the extrusion process [20,21]. In addition, the coarse net-like phases turn into small particles, which distribute between the boundary of β-Li grains or the boundary of β-Li and α-Mg.

XRD patterns in Fig. 4 show the phase compositions of the alloys before and after extrusion. It confirms that all of the as-cast and as-extruded alloys mainly consist of α-Mg, β-Li, W-phase, Mg_3Gd, and MgLiZn phases [5,11,22−24]. Due to the sensitivity limit of XRD, the peaks of other phases are not detected. The matrix is made up of α-Mg and β-Li, which is consistent with the typical duplex structure in the above optical micrographs. Figure 4(a) shows that the alloys with Zn/Gd mass ratio of 4 have a higher peak value of W-phase. Figure 4(b) indicates that the number of diffraction peaks decreases after extrusion, but the variety of phases stays unchanged. Figure 5 shows the SEM images of the as-extruded alloys parallel

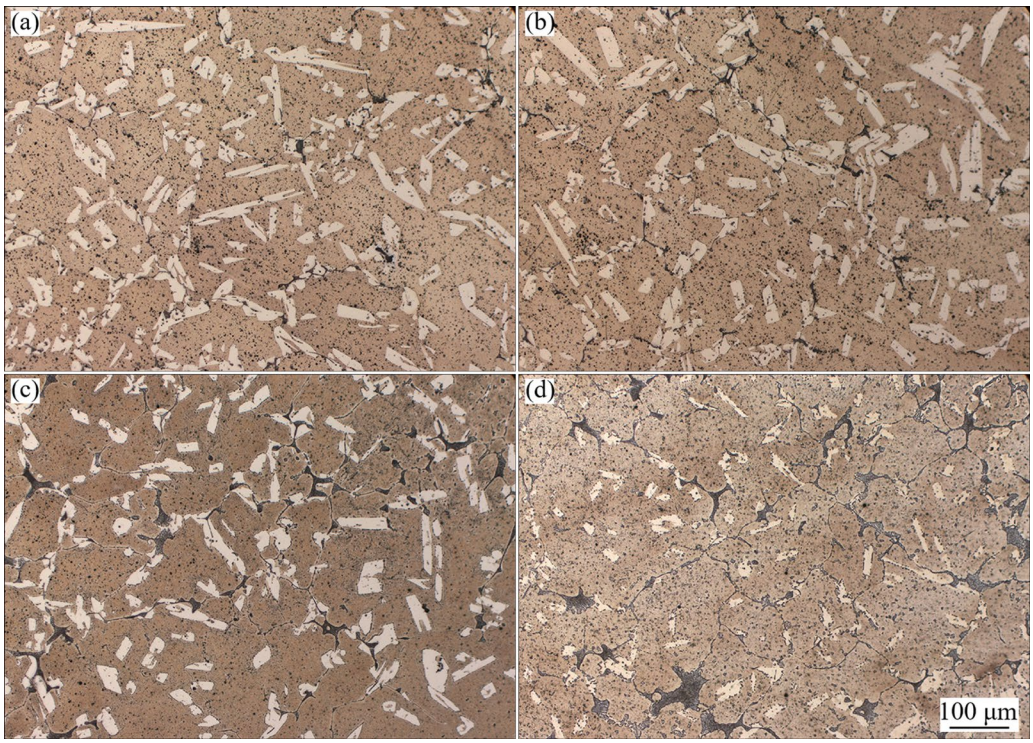

Fig. 1 Optical micrographs of as-cast alloys: (a) Alloy I; (b) Alloy II; (c) Alloy III; (d) Alloy IV

Table 2 Average grain sizes of α-Mg grains in as-cast Mg−Li−Zn−Gd alloys

Alloy No.	Zn/Gd mass ratio	Average grain size/μm
I	2	67
II	4	54
III	4	50
IV	4	36

to the extrusion direction. After hot extrusion, most of the second phases are cracked into small particles. The precipitates are distributed in a streamline along the extrusion direction. The grain boundaries of the β-Li grains can be seen in Figs. 5(c) and (d), which also proves that dynamic recrystallization occurs during the hot extrusion process [25,26].

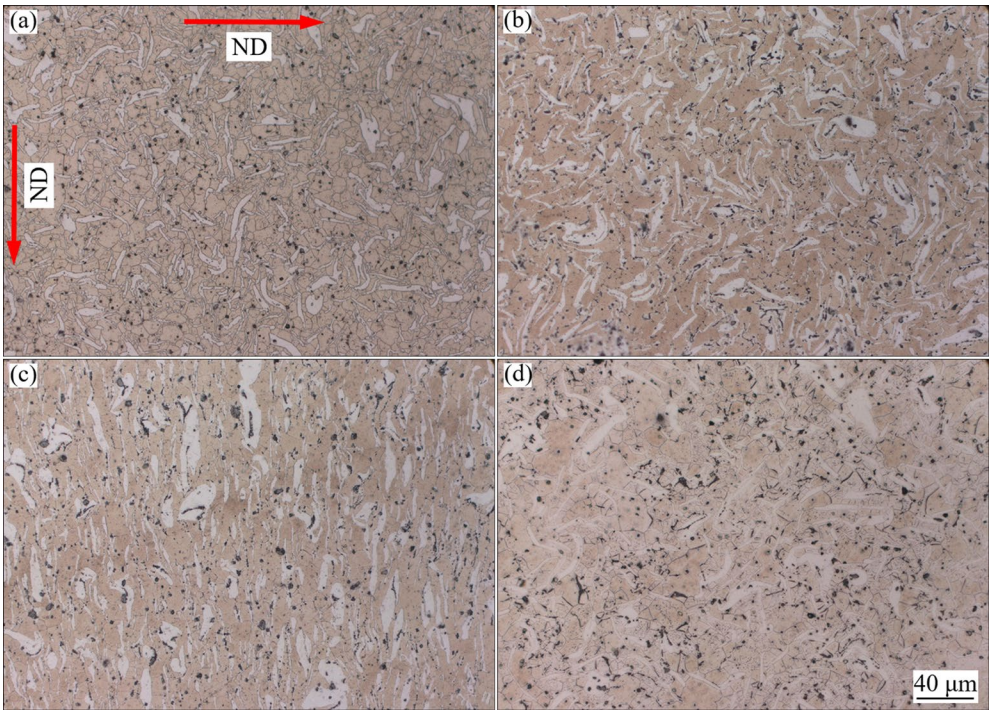

Fig. 2 Optical micrographs of as-extruded alloys perpendicular to extrusion direction (Normal direction, ND): (a) Alloy I; (b) Alloy II; (c) Alloy III; (d) Alloy IV

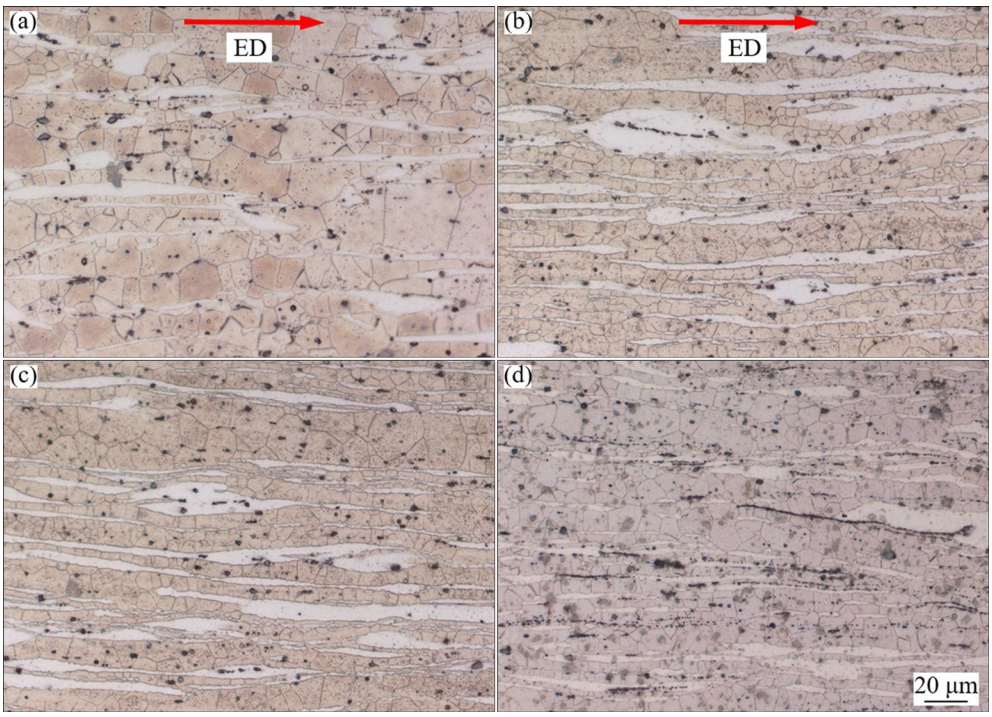

Fig. 3 Optical micrographs of as-extruded alloys parallel to extrusion direction (ED): (a) Alloy I; (b) Alloy II; (c) Alloy III; (d) Alloy IV

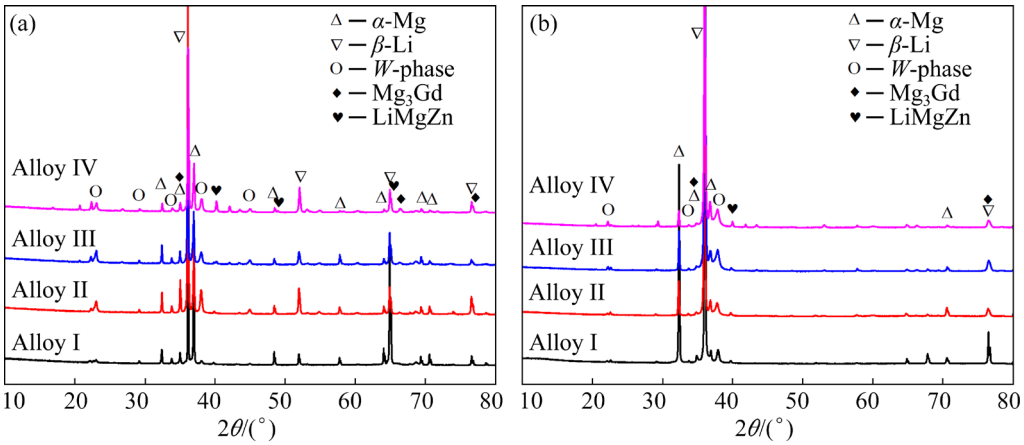

Fig. 4 XRD patterns of as-cast (a) and as-extruded (b) Mg−Li−Zn−Gd alloys

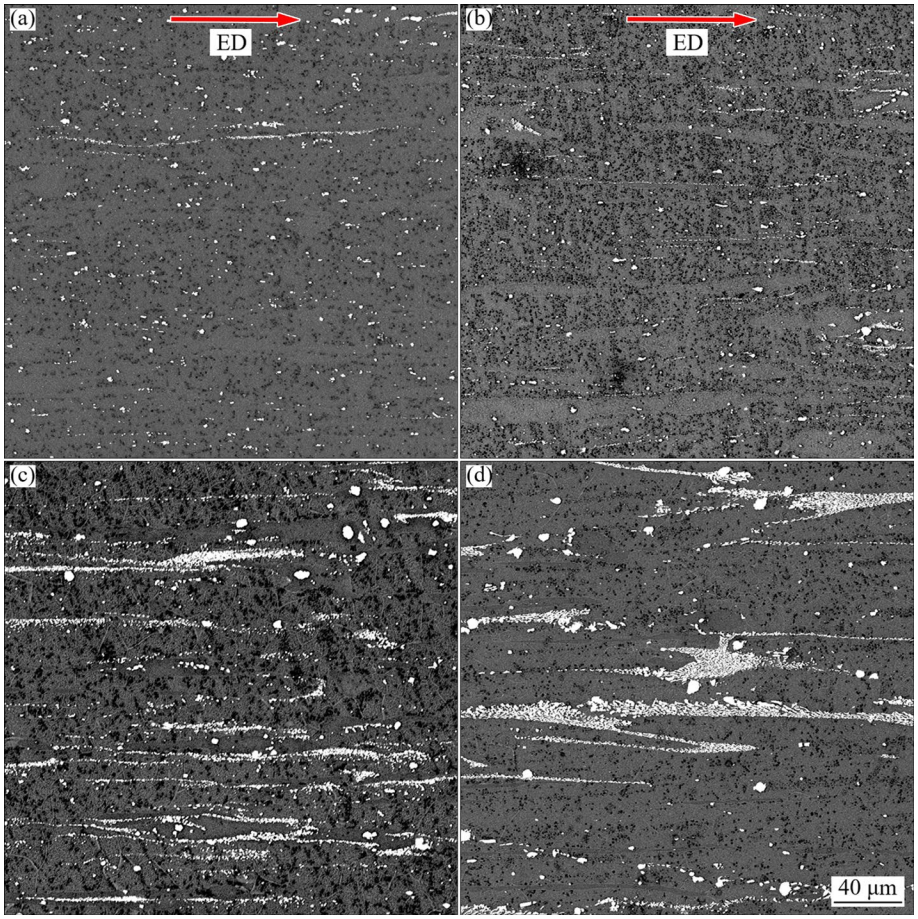

Fig. 5 SEM micrographs of as-extruded alloys parallel to extrusion direction: (a) Alloy I; (b) Alloy II; (c) Alloy III; (d) Alloy IV

Figure 6 shows the SEM images of the as-extruded alloys perpendicular to the extrusion direction. Many tiny particles are exhibited in Fig. 6(a) and the hollow-skeleton-like phases exist in Figs. 6(b−d). In addition, incompletely broken bulky phases exist in Fig. 6(d). The EDS results of the points marked in Fig. 6 are listed in Table 3. Combined with XRD results, it can be determined that the particles marked with 5, 8, and 11 are Mg_3Gd phase. The particles marked with 1, 3, 4, 6, 9, 12, and 13 are *W*-phase (the Zn/Gd mass ratio is about 1.5). Since the Li element is not visible in the EDS map, it can be judged that the particles marked with 2, 7, 10, and 14 are MgLiZn phases. These MgLiZn particles are small in size about 1 μm.

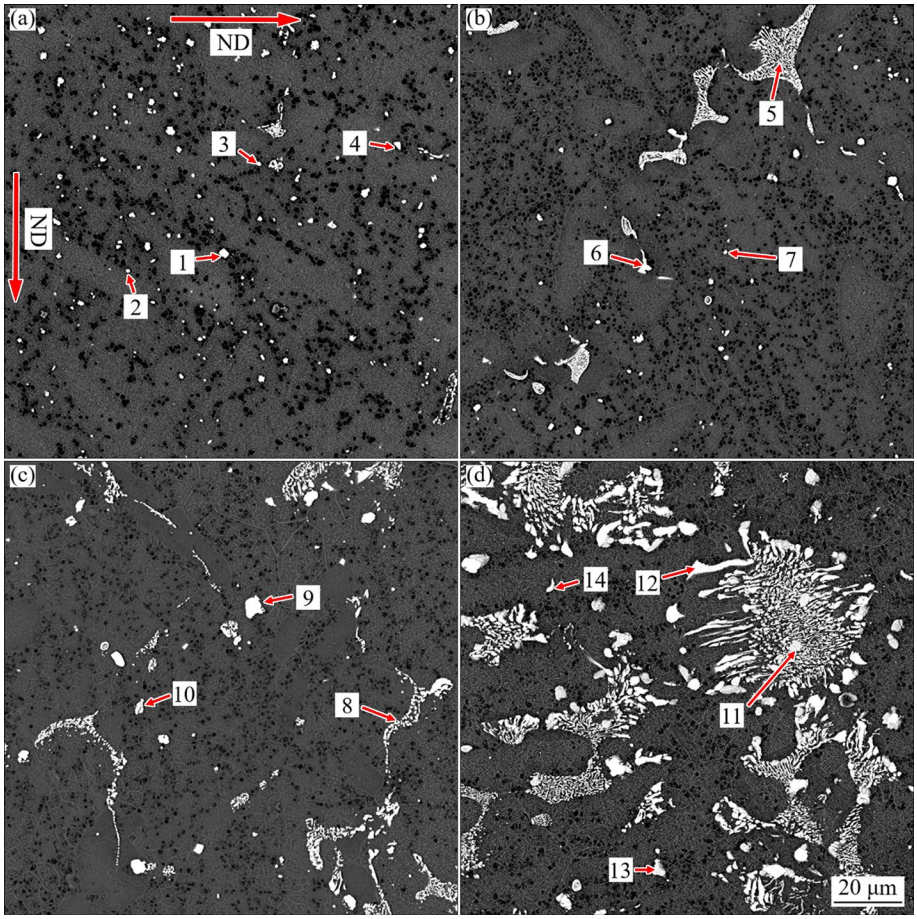

Fig. 6 SEM micrographs of as-extruded alloys perpendicular to extrusion direction: (a) Alloy I; (b) Alloy II; (c) Alloy III; (d) Alloy IV

Table 3 EDS point scan analysis results for positions in Fig. 6

Point No.	Content/at.%		
	Mg	Zn	Gd
1	89.21	6.23	4.56
2	86.24	13.76	–
3	89.73	5.72	4.54
4	78.48	12.16	9.35
5	61.69	–	38.31
6	89.44	6.58	3.98
7	68.36	31.40	0.24
8	69.03	–	30.97
9	91.72	5.43	2.85
10	76.14	13.86	–
11	72.39	–	27.61
12	87.56	8.21	4.23
13	82.26	11.6	6.14
14	87.30	12.70	–

The TEM equipment is employed to observe the microstructure morphology and identify the second phase by SAED pattern. As shown in Fig. 7, abundant spherical particles with a size of about 100 nm are widely distributed in the β-Li matrix. It can be inferred that these spherical particles only exist in the β-Li phase or along the boundary of α-Mg and β-Li phases. Figure 8 shows the TEM micrographs of the as-extruded Alloy IV. Figures 8(a) and (b) show that the second phase is mainly distributed along the grain boundary. As shown in Fig. 8(c), the *W*-phase is the bcc structure with an elliptical shape. EDS results indicate that the chemical compositions include 70.61 at.% Mg, 18.53 at.% Zn and 10.86 at.% Gd. The lattice parameter of the *W*-phase is calculated as 7.168 Å. Fig. 8(d) indicates that the $MgZn_2$ phase with hcp structure presents an irregular polygon, with a size of about 2 μm. From Figs. 8(e) and (f), both the Mg_3Gd phase and MgLiZn phase have a bcc structure. Figure 9(a) shows the bright field TEM image of the as-extruded Alloy IV. Figures 9(b) and

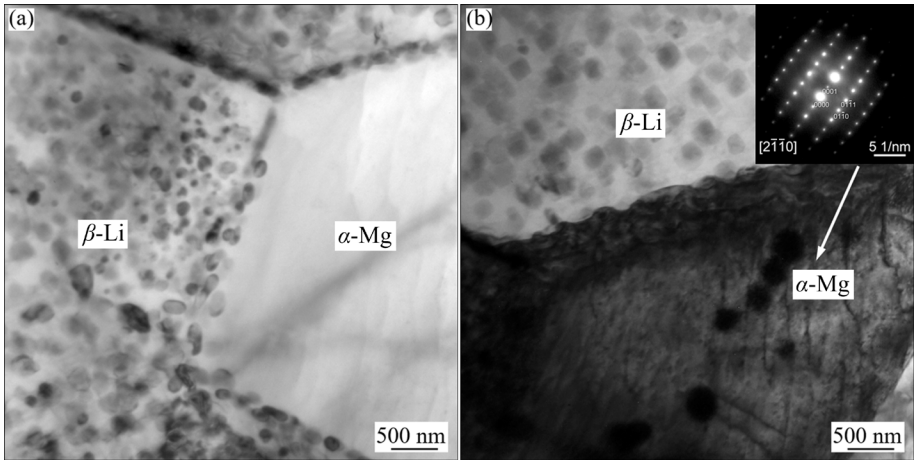

Fig. 7 TEM micrographs of dual matrix phases in as-extruded Alloy IV: (a) Dispersed spherical particles with size of about 100 nm precipitated in β-Li matrix; (b) α-Mg matrix phase and corresponding SAED patterns

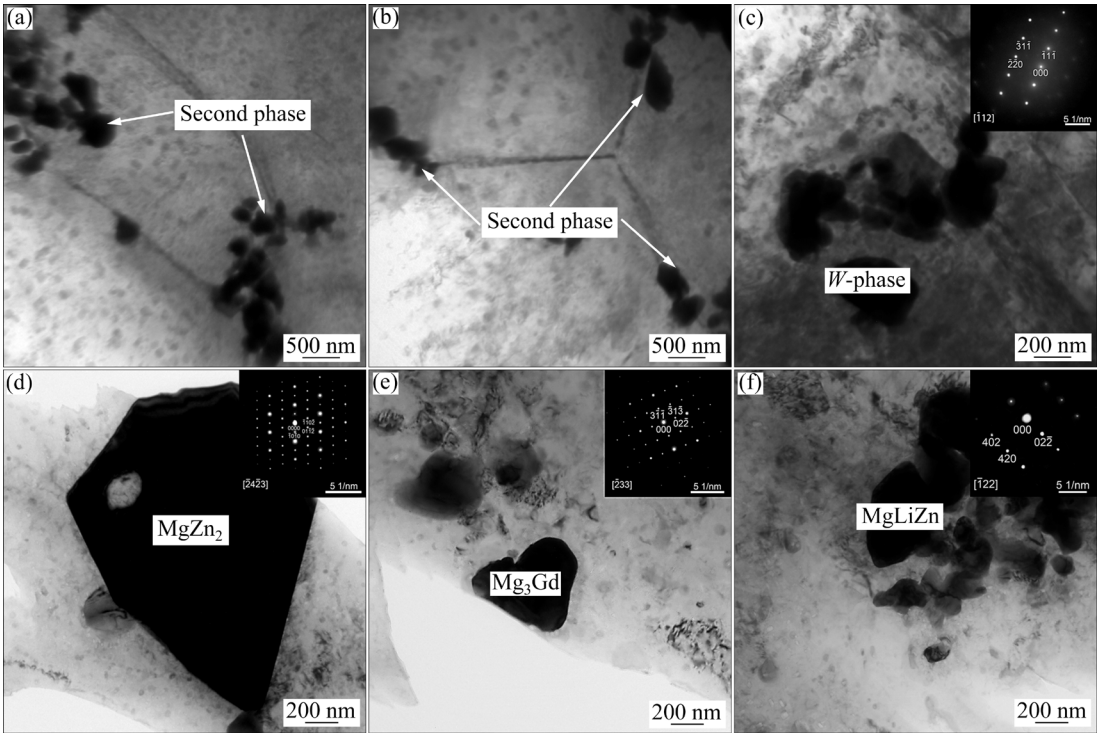

Fig. 8 TEM micrographs of second phases in as-extruded Alloy IV: (a) Distribution of second phases; (b) Second phases distributed along grain boundary; (c) *W* phase; (d) $MgZn_2$ phase; (e) Mg_3Gd phase; (f) MgLiZn phase

(c) show the dark field TEM images of the MgLiZn phase and Fig. 9(d) shows the dark field TEM image of the β-Li matrix. It can be inferred that the MgLiZn phases are also distributed in the β-Li phase or along the boundary.

3.2 Tensile properties and fracture behavior of as-cast and as-extruded Mg−Li−Zn−Gd alloys

Tensile properties of the Mg−Li−Zn−Gd alloys before and after extrusion are measured. The comparison of mechanical properties of the as-cast and as-extruded alloys is shown in Figs. 10 and 11, respectively. The typical tensile stress−strain curves of the as-extruded Mg−Li−Zn−Gd alloys are shown in Fig. 12. In Fig. 10, the yield strength (YS) and ultimate tensile strength (UTS) of the as-cast Mg−Li−Zn−Gd alloys increase with the increase of Zn and Gd contents. The as-cast Alloy IV has the highest yield strength and tensile strength of 193 and 237 MPa, respectively. After extrusion deformation, the strength of the alloys is improved

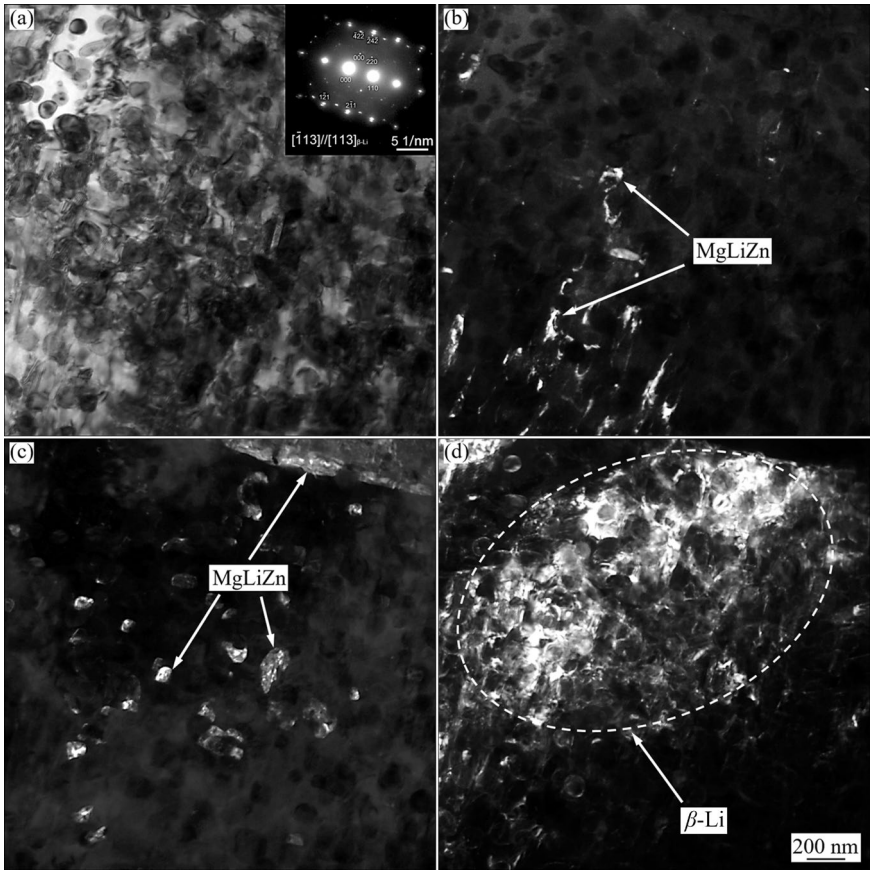

Fig. 9 Bright and dark field TEM micrographs of as-extruded Alloy IV: (a) Bright field; (b) Dark field of MgLiZn within β-Li phase; (c) Dark field of MgLiZn at grain boundary of dual matrix phases and within β-Li phase; (d) Dark field of β-Li

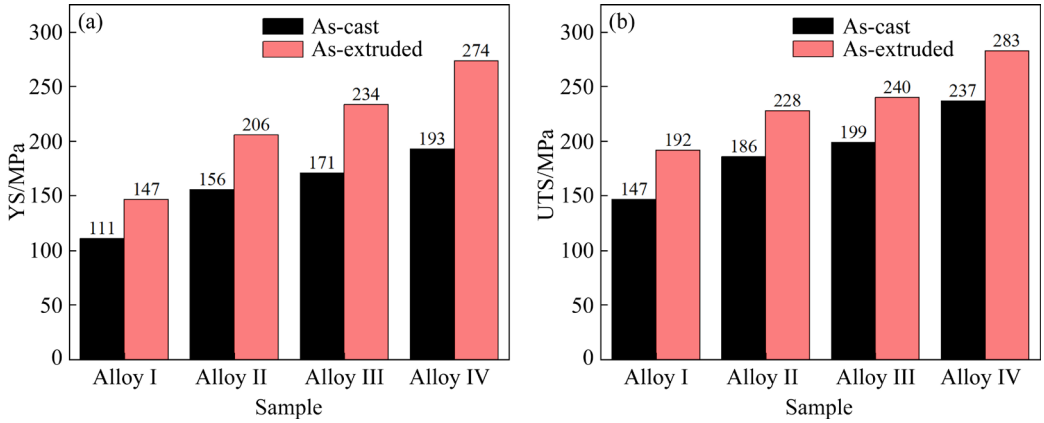

Fig. 10 Comparison of yield strength (a) and ultimate tensile strength (b) between as-cast and as-extruded Mg−Li−Zn−Gd alloys

greatly. The yield strength increment (ΔYS) increases with the increase of Zn and Gd contents. And the ΔYS of Alloy I with the Zn/Gd mass ratio of 2 is less than that of other alloys with the Zn/Gd mass ratio of 4. Compared with the ΔYS, the ultimate tensile strength increment (ΔUTS) of the alloys with different Zn and Gd contents after extrusion deformation has little difference. The average ΔUTS of the as-extruded alloys is 43.5 MPa compared with the as-cast alloys. Therefore, with the increase of Zn and Gd contents, the difference between YS and UTS of the as-extruded alloys decreases. The as-extruded Alloy IV has the highest YS and UTS of 274 and 283 MPa, respectively. In Fig. 12, the elongation of the as-cast alloys decreases with the increase of Zn

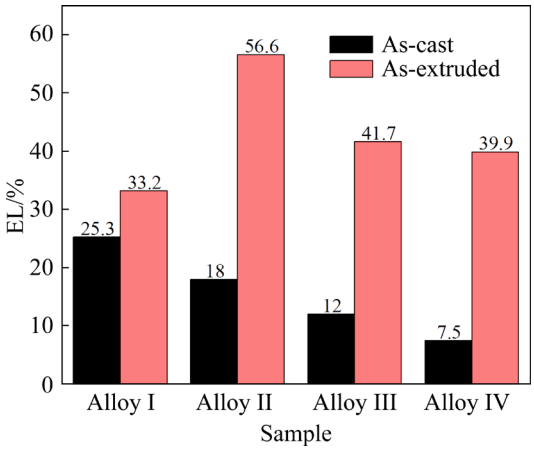

Fig. 11 Comparison of elongation between as-cast and as-extruded Mg−Li−Zn−Gd alloys

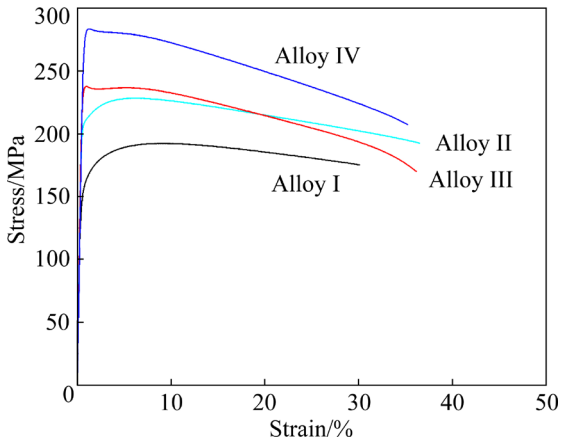

Fig. 12 Typical tensile stress−strain curves of as-extruded alloys

and Gd contents. After extrusion, the elongation of all alloys increases. But there is no clear rule between the elongation increment (ΔEL) and the contents of Zn and Gd. In a word, the strength and plasticity of the alloys have been greatly improved after extrusion. The ΔUTS is not related to the contents of Zn and Gd. The ΔYS is positively related to the contents of Zn and Gd.

Figure 13 shows the tensile fracture surface of the as-extruded Mg−Li−Zn−Gd alloys. It can be seen from Fig. 13 that, there are a large number of dimples in the fracture surface of all as-extruded alloys. It is the typical ductile fracture mode, which is consistent with the good plasticity of the as-extruded Mg−Li−Zn−Gd alloys in Fig. 12. Broken second phase particles can be seen at the bottom of the dimple. These particles may be the source of fracture during tensile deformation [25]. After extrusion, the precipitated phase in the alloys deforms under the action of extrusion force, and the

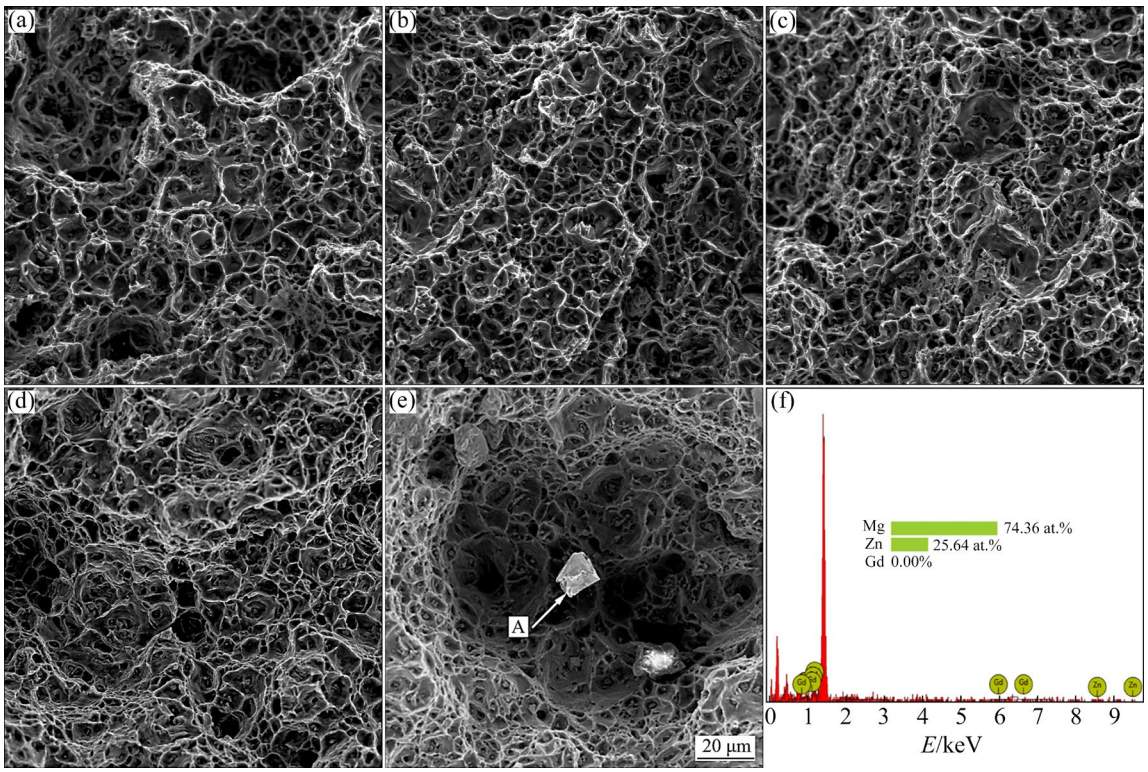

Fig. 13 SEM images showing tensile fracture surfaces of as-extruded alloys: (a) Alloy I; (b) Alloy II; (c) Alloy III; (d) Alloy IV; (e) $MgZn_2$ particle on fracture surface of Alloy I; (f) EDS pointing analysis results of Particle A in (e)

large second phase has been broken [23−25]. Therefore, it is necessary to identify and analyze the particles at the bottom of the dimple on the fracture surface of the as-extruded alloys. Figure 13(f) shows the EDS point scan analysis results of irregular and coarse particles at the bottom of a dimple of Alloy I with the worst plasticity after extrusion. In Fig. 13(e), the broken Particle A at the dimple mainly contains Mg and Zn. The molar ratio of Mg to Zn is about 3:1. Considering the influence of Mg atoms in the matrix, the Mg/Zn molar ratio is high. Combined with the Mg−Zn binary phase diagram, it can be inferred that Particle A is the $MgZn_2$ phase. The $MgZn_2$ phase has been observed in TEM, as shown in Fig. 8(d). As a phase with an hcp structure, the $MgZn_2$ phase has few slip systems and poor plasticity, which is easy to become the fracturing source of the as-extruded alloys.

4 Discussion

4.1 Effect of Zn and Gd contents on microstructures of Mg−Li−Zn−Gd alloys

Through investigating the microstructure of the Mg−Li−Zn−Gd alloys with the Zn/Gd mass ratios of 2 and 4, the effects of Zn and Gd contents on the microstructure evolution are analyzed. Figure 14 illustrates the schematic diagram of the precipitate evolution in the Mg−Li−Zn−Gd alloy during extrusion. With the increase of Zn and Gd contents, the network-like phases appear and gradually coarsen. Results also show that the addition of Zn and Gd elements can refine α-Mg grains [27]. The average grain size of α-Mg in Alloy IV is about 36 μm. According to the XRD patterns, the as-cast alloy mainly consists of α-Mg, β-Li, MgLiZn, Mg_3Gd, and W-phase.

The type of phases remains unchanged after extrusion. A large number of fine equiaxed grains appear in the β-Li phase of as-extruded alloy, indicating that dynamic recrystallization occurs during extrusion [27−29]. There are also some larger equiaxed β-Li grains in Alloys I−III, which may have grown after dynamic recrystallization. With the increase of Zn and Gd contents, the recrystallized β-Li grains become more uniform and finer. There are few larger equiaxed β-Li grains in Alloy IV. A large number of precipitated particles in the β-Li matrix phase or at the β-Li grain boundary provide more nucleation sites, which limits the growth of recrystallized grains [30,31]. The α-Mg matrix phase is stretched into long strips along the extrusion direction. The bi-modal structure is formed after extrusion, which consists stretched coarse-grain region with a strong extrusion texture (long-strip-like α-Mg matrix phase) and recrystallization fine-grain region (equiaxed β-Li matrix phase) [32,33].

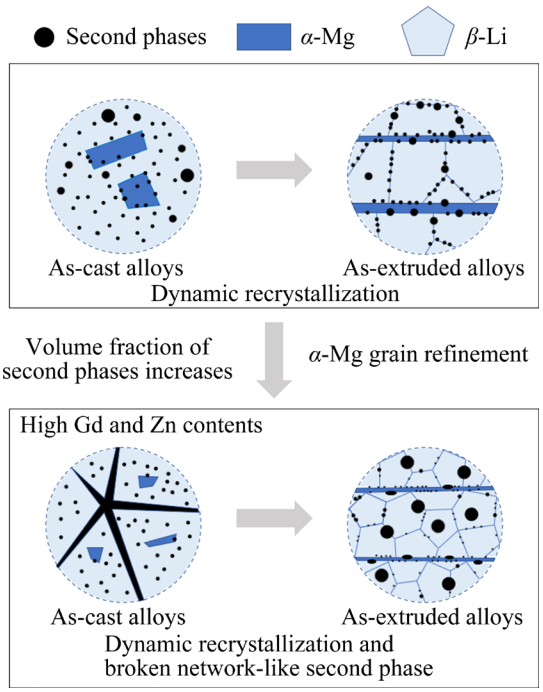

Fig. 14 Schematic diagram illustrating precipitate evolution during extrusion

With the increase of Zn and Gd contents, the volume fraction of the second phases increases obviously, and the size of the cracked second phase increases as well. The hollow-skeleton-like Mg_3Gd phases have a large size of 10−20 μm. The size of the MgLiZn particles in the as-extruded alloys is small, about 1 μm, which is mainly dispersed in the β-Li phase. The solid solubility of Zn in the α-Mg phase is low, and more Zn is provided to the Mg−Li−Zn phase in the β-Li phase matrix for precipitation and growth [34]. The W-phase is mainly distributed along the grain boundary in the as-extruded alloy, which has a larger size (5−10 μm) than the MgLiZn phase by SEM analysis. A very fine spherical particle is found dispersed in the β-Li phase with a size of about 100 nm. After extrusion, the W-phase and MgLiZn particles are fully broken, while only a part of the hollow-skeleton-like Mg_3Gd phases are broken [29].

4.2 Strengthening mechanism in as-extruded Mg−Li−Zn−Gd alloys

In this work, the mechanical properties of the as-extruded Mg−Li−Zn−Gd alloys with the Zn/Gd mass ratios of 2 and 4 are studied. The results show that the strength and plasticity of the alloys have been greatly improved after extrusion. With the increase of Zn and Gd contents, the YS and UTS of the as-extruded alloys increase. Besides, it is shown that ΔYS of the alloy with high Zn and Gd contents and high Zn/Gd mass ratio after hot extrusion deformation is greater than ΔUTS so that the material potential of the alloy can be fully exploited. The as-extruded Mg−8Li−8Zn−2Gd alloy exhibits the best mechanical properties with the YS of 274 MPa, UTS of 283 MPa, and EL of 39.9%. The main strengthening mechanism of the as-extruded Mg−Li−Zn−Gd alloys is analyzed.

Firstly, after extrusion deformation, fine equiaxed recrystallized grains are formed because of the dynamic recrystallization of *β*-Li, which results in fine grain strengthening [23−26,35]. Micron-size *β*-Li grains conform to the Hall–Petch relationship, which shows that as the grain size decreases, the strength of the alloy increases [35]. The recrystallized *β*-Li grains of Alloy IV are more uniform and finer, which provides a better grain-refinement strengthening effect.

As seen in Fig. 3, the bi-modal structure consisting of the recrystallized fine-grain region and stretched coarse-grain region is formed after extrusion, which can also strengthen the alloy [33]. The stretched coarse grain (long-strip-like *α*-Mg matrix phase) with a strong extrusion texture has a good texture-strengthening effect [33]. Fine recrystallized grains (equiaxed *β*-Li matrix phase) acted as the lubricant between stretched coarse grains, which guarantees good ductility while improving strength [33].

Generally, the factors contributing to the YS of an Mg alloy mainly consist of the friction stress of pure Mg, solid-solution strengthening, precipitation strengthening, grain-refinement strengthening, and texture strengthening [32,33]. After extrusion, the concentration of solute and volume fraction of the second phase is almost the same as those of the as-cast alloy. Therefore, the fine-grained strengthening of recrystallized *β*-Li phase and texture strengthening of extruded *α*-Mg phase contribute greatly to the strength of the alloy.

Secondly, it is concluded that with increasing the Zn and Gd contents in Mg−Li alloys, the number of the second phase increases, and the average size of the particle phase also increases. The strengthening effect of the second phase is related to the type, shape, size, quantity, and distribution of the second phase [28,29,34]. Most of the second phases are broken after extrusion, which has a very excellent dispersion-strengthening effect on the alloy. The Alloy IV with the largest number of the second phases has the best strengthening effect.

The TEM observation in Fig. 7 shows that there are spherical particles with a size of only about 100 nm uniformly distributed in the *β*-Li matrix phase and the grain boundary. According to previous research, it can be inferred that the spherical particles might be MgLiZn phase [28,29,34]. The high-density spherical second phase particles distributed in the *β*-Li matrix phase can inhibit dislocation transfer and movement within the grains, which can strengthen the alloy matrix [30,31,34,36,37]. Both the *W*-phase and MgLiZn phase are effective strengthening phases in Mg−Li alloys [26]. The *W*-phase and MgLiZn particles with a size of several microns mainly distributed at the grain boundary can reinforce alloys by pinning the grain boundary and hindering dislocation motion [30,31]. Besides, the *W*-phase can promote recrystallization by regulating their morphology and size which have a significant effect on fine-grain and dispersion strengthening [30]. The irregular polygonal $MgZn_2$ particles with an hcp structure have few slip systems and poor plasticity. As shown in Fig. 13(e), as a hard brittle phase, the large-sized $MgZn_2$ phase is easy to become the crack source of the as-extruded alloys, which is bad for the plasticity and strength of the alloy.

5 Conclusions

(1) The as-cast and as-extruded Mg−Li−Zn−Gd alloys mainly consist of *α*-Mg, *β*-Li, *W*-phase, Mg_3Gd, and MgLiZn phases. The addition of Zn and Gd could refine the *α*-Mg grains. Besides, with the increase of Zn and Gd, the number of the second phase increases.

(2) After extrusion deformation, the bi-modal structure is formed, which consists of the stretched coarse-grain region (long-strip-like *α*-Mg phase)

and recrystallization fine-grain region (equiaxed β-Li phase). The W-phase and MgLiZn phase are fully broken after extrusion with a size of several microns. The spherical particles are found in the β-Li with a size of only about 100 nm.

(3) The strength and plasticity of the alloys are greatly improved after extrusion. The YS and UTS of the as-extruded alloys increase with the increase of Zn and Gd contents. The Mg−8Li−8Zn−2Gd alloy exhibits the best mechanical properties with the YS of 274 MPa, UTS of 283 MPa, and EL of 39.9%.

(4) The main strengthening mechanisms of the as-extruded Mg−Li−Zn−Gd alloy are as follows: the bi-modal structure strengthening which consists of the fine crystal strengthening of recrystallized β-Li and texture strengthening of long-strip-like α-Mg, and the dispersion strengthening of the spherical particles and the broken second phases.

CRediT authorship contribution statement

Yu-chuan HUANG: Conceptualization, Methodology, Investigation, Formal analysis, Writing − Original draft; **Quan-da ZHANG:** Investigation, Writing − Review & editing, Validation; **Si-jie OUYANG:** Investigation; Resources; **Fu-zhen SUN:** Writing − Review & editing, Validation; **Jia-wei SUN:** Writing − Review & editing, Validation; **Hui-yu LI:** Investigation, Visualization; **Guo-hua WU:** Supervision; **Pei-jun CHEN:** Supervision; **Wen-cai LIU:** Supervision, Project administration, Writing − Review & editing, Funding acquisition.

Declaration of competing interest

The authors declare that they have no known competing financial interests or personal relationships that could have appeared to influence the work reported in this paper.

Declaration of interests

The authors declare that they have no known competing financial interests or personal relationships that could have appeared to influence the work reported in this paper.

Acknowledgments

This work is supported by the Open Fund of State Key Laboratory of Advanced Forming Technology and Equipment (No. SKL202005), the Major Scientific and Technological Innovation Project of Luoyang, China (No. 2201029A), the National Natural Science Foundation of China (Nos. 51771115, 51775334), and the Research Program of SAST-SJTU Joint Research Center of Advanced Spaceflight Technologies, China (No. USCAST2020-14).

References

[1] WU Rui-zhi, YAN Yong-de, WANG Gui-xiang, MURR L E, HAN Wei, ZHANG Zhong-wu, ZHANG Mi-lin. Recent progress in magnesium−lithium alloys [J]. International Materials Reviews, 2015, 60(2): 65−100.

[2] PARK G H, KIM J T, PARK H J, KIM Y S, JEONG H J, LEE N, SEO Y, SUH J Y, SON H T, WANG W M, PARK J M, KIM K B. Development of lightweight Mg−Li−Al alloys with high specific strength [J]. Journal of Alloys and Compounds, 2016, 680: 116−120.

[3] KIM Y H, KIM J H, YU H S, CHOI J W, SON H T. Microstructure and mechanical properties of Mg−xLi−3Al−1Sn−0.4Mn alloys (x=5, 8 and 11 wt.%) [J]. Journal of Alloys and Compounds, 2014, 583: 15−20.

[4] CHEN Zhao-yun, LI Zhi-qiang, YU Chun. Hot deformation behavior of an extruded Mg–Li–Zn–RE alloy [J]. Materials Science and Engineering A, 2011, 528(3): 961−966.

[5] JI Hao, LIU Wen-cai, WU Guo-hua, OUYANG Si-jie, GAO Zhan-kui, PENG Xiang, DING Wen-jiang. Influence of Er addition on microstructure and mechanical properties of as-cast Mg−10Li−5Zn alloy [J]. Materials Science and Engineering A, 2019, 739(2): 395−403.

[6] CHEN Zhao-yun, DONG Zi-chao, YU Chun, TONG Rui. Microstructure and properties of Mg−5.21Li−3.44Zn−0.32Y−0.01Zr alloy [J]. Materials Science and Engineering A, 2013, 559(1): 651−654.

[7] BAE D H, KIM S H, KIM D H, KIM W T. Deformation behavior of Mg−Zn−Y alloys reinforced by icosahedral quasicrystalline particles [J]. Acta Materialia, 2002, 50(9): 2343−2356.

[8] XU Dao-kui, LIU Lu, XU Yong-bo, HAN En-hou. Effect of microstructure and texture on the mechanical properties of the as-extruded Mg−Zn−Y−Zr alloys [J]. Materials Science and Engineering A, 2007, 443(1/2): 248−256.

[9] HUANG Hua, YUAN Guang-yin, CHU Zhen-hua, DING Wen-jiang. Microstructure and mechanical properties of double continuously extruded Mg−Zn−Gd-based magnesium alloys [J]. Materials Science and Engineering A, 2013, 560: 241−248.

[10] ZHANG Yang, ZHANG Jie, WU Guo-hua, LIU Wen-cai, ZHANG Liang, DING Wen-jiang. Microstructure and tensile properties of as-extruded Mg–Li–Zn–Gd alloys reinforced with icosahedral quasicrystal phase [J]. Materials & Design, 2015, 66: 162−168.

[11] XU Dao-kui, TANG Wei-neng, LIU Lu, XU Yong-bo, HAN En-hou. Effect of Y concentration on the microstructure and mechanical properties of as-cast Mg−Zn−Y−Zr alloys [J]. Journal of Alloys and Compounds, 2007, 432(1/2): 129−134.

[12] WANG Qing-feng, LIU Ke, WANG Zhao-hui, LI Shu-bo, DU Wen-bo. Microstructure, texture, and mechanical properties of as-extruded Mg−Zn−Er alloys containing W-phase [J]. Journal of Alloys and Compounds, 2014, 602: 32−39.

[13] ZHANG Ya, ZENG Xiao-qin, LIU Liu-fa, LU Chen, ZHOU Han-tao, LI Qiang, ZHU Yan-ping. Effects of yttrium on microstructure and mechanical properties of hot-extruded Mg−Zn−Y−Zr alloys [J]. Materials Science and Engineering A, 2004, 373(1/2): 320−327.

[14] LEE J Y, KIM D H, LIM H K, KIM D H. Effects of Zn/Y ratio on microstructure and mechanical properties of Mg−Zn−Y alloys [J]. Materials Letters, 2005, 59(29/30): 3801−3805.

[15] XU Dao-kui, LIU Lu, XU Yong-bo, HAN En-hou. The influence of element Y on the mechanical properties of the as-extruded Mg−Zn−Y−Zr alloys [J]. Journal of Alloys and Compounds, 2006, 426(1/2): 155−161.

[16] MENG Xiang-rui, WU Rui-zhi, ZHANG Mi-lin, WU Li-bin, CUI Chong-liang. Microstructures and properties of superlight Mg−Li−Al−Zn wrought alloys [J]. Journal of Alloys and Compounds, 2009, 486(1/2): 722−725.

[17] ZHANG Jie, ZHANG Yang, WU Guo-hua, LIU Wen-cai, ZHANG Liang, DING Wen-jiang. Microstructure and mechanical properties of as-cast and extruded Mg−8Li−3Al−2Zn−0.5Nd alloy [J]. Materials Science and Engineering A, 2015, 621: 198−203.

[18] ZHAO Jiong, LI Zhong-quan, LIU Wen-cai, ZHANG Jie, ZHANG Liang, TIAN Ying, WU Guo-hua. Influence of heat treatment on microstructure and mechanical properties of as-cast Mg−8Li−3Al−2Zn−*x*Y alloy with duplex structure [J]. Materials Science and Engineering A, 2016, 669: 87−94.

[19] ZHAO Jiong, ZHANG Jie, LIU Wen-cai, WU Gua-hua, ZHANG Liang. Effect of Y content on microstructure and mechanical properties of as-cast Mg−8Li−3Al−2Zn alloy with duplex structure [J]. Materials Science and Engineering A, 2016, 650: 240−247.

[20] LIU Yong, YUAN Guang-yin, ZHANG Song, ZHANG Xin-ping, LU Chen, DING Wen-jiang. Effects of Zn/Gd ratio and content of Zn, Gd on phase constitutions of Mg alloys [J]. Materials Transactions, 2008, 49(5): 941−944.

[21] CHANG T C, WANG J Y, CHU C L, LEE S. Mechanical properties and microstructures of various Mg−Li alloys [J]. Materials Letters, 2006, 60(27): 3272−3276.

[22] KARAMI M, MAHMUDI R. The microstructural, textural, and mechanical properties of extruded and equal channel angularly pressed Mg−Li−Zn alloys [J]. Metallurgical and Materials Transactions A, 2013, 44(8): 3934−3946.

[23] LIU Yong, YUAN Guang-yin, LU Chen, DING Wen-jiang. Stable icosahedral phase in Mg−Zn−Gd alloy [J]. Scripta Materialia, 2006, 55(10): 919−922.

[24] XU Dao-kui, TANG Wei-neng, LIU Lu, XU Yong-bo, HAN En-hou. Effect of W-phase on the mechanical properties of as-cast Mg−Zn−Y−Zr alloys [J]. Journal of Alloys and Compounds, 2008, 461(1): 248−252.

[25] YAMASAKI M, ANAN T, YOSHIMOTO S, KAWAMURA Y. Mechanical properties of warm-extruded Mg−Zn−Gd alloy with coherent 14H long periodic stacking ordered structure precipitate [J]. Scripta Materialia, 2005, 53(7): 799−803.

[26] XU Dao-kui, ZU Ting-ting, YIN Miao, XU Yong-bo, HAN En-hou. Mechanical properties of the icosahedral phase reinforced duplex Mg−Li alloy both at room and elevated temperatures [J]. Journal of Alloys and Compounds, 2014, 582: 161−166.

[27] WANG Xue-zhao, WANG You-qiang, NI Chen-bing, FANG Yu-xin, YU Xiao, ZHANG Ping. Effect of Gd content on microstructure and dynamic mechanical properties of solution-treated Mg−*x*Gd−3Y−0.5Zr alloy) [J]. Transactions of Nonferrous Metals Society of China, 2022, 32(7): 2177−2189.

[28] JI Hao, WU Guo-hua, LIU Wen-cai, SUN Jiang-wei, DING Wen-jiang. Role of extrusion temperature on the microstructure evolution and tensile properties of an ultralight Mg−Li−Zn−Er alloy [J]. Journal of Alloys and Compounds, 2021, 876: 160181.

[29] OUYANG Si-jie, LIU Wen-cai, WU Guo-hua, JI Hao, GAO Zhan-kui, PENG Xiang, LI Zhong-quan, DING Wen-jiang. Microstructure and mechanical properties of as-cast Mg−8Li−*x*Zn−*y*Gd (x=1, 2, 3, 4; y=1, 2) alloys [J]. Transactions of Nonferrous Metals Society of China, 2019, 29(6): 1211−1222.

[30] XIE Jin-shu, ZHANG Jing-huai, YOU Zi-hao, LIU Shu-juan, GUAN Kai, WU Rui-zhi, WANG Jun, FENG Jing. Towards developing Mg alloys with simultaneously improved strength and corrosion resistance via RE alloying [J]. Journal of Magnesium and Alloys, 2021, 9(1): 41−56.

[31] ZHANG Jing-huai, LIU Shu-juan, WU Rui-zhi, HOU Le-gan, ZHANG Mi-lin. Recent developments in high-strength Mg−RE-based alloys: Focusing on Mg−Gd and Mg−Y systems [J]. Journal of Magnesium and Alloys, 2018, 6(3): 277−291.

[32] WEI Guo-bing, PENG Xiao-dong, HU Fa-ping, HADADZADEH A, YANG Yan, XIE Wei-dong, WELLS M A. Thermal deformation behavior and constitutive model of dual-phase Mg−Li alloy [J]. Transactions of Nonferrous Metals Society of China, 2016, 26(02): 508−518.

[33] HONG Min, SHAH S S, WU Di, CHEN Rong-shi, DU Xing-hao, HU Nan-tao, ZHANG Ya-fei. Ultra-high strength Mg−9Gd−4Y−0.5Zr alloy with bi-modal structure processed by traditional extrusion [J]. Metals and Materials International, 2016, 22(6): 1091−1097.

[34] JI Hao, WU Guo-hua, LIU Wen-cai, ZHANG Xiao-long, ZHANG Liang, WANG Ming-xu. Origin of the age-hardening and age-softening response in Mg−Li−Zn based alloys [J]. Acta Materialia, 2022, 226: 117673.

[35] ZHANG Zhi, ZHANG Jing-huai, WANG Jun, LI Ze-hua, XIE Jin-shu, LIU Shu-juan, GUAN Kai, WU Rui-zhi. Toward the development of Mg alloys with simultaneously improved strength and ductility by refining grain size via the deformation process [J]. International Journal of Minerals, Metallurgy and Materials volume, 2021, 28(1): 30−45.

[36] LOU Wei-xin, XIE Hong-bo, ZHAO Xiao-bo, BAI Jun-yuan, ZHANG He-hang, WANG Yi, LI Xin-ze, PAN Hu-cheng, REN Yu-ping, QIN Gao-wu. Variable precipitation behaviors of Laves phases in an ultralight Mg−Li−Zn alloy [J]. Journal of Magnesium and Alloys, 2023, 11: 2018−2026.

[37] PENG Xiang, SUN Jia-wei, LIU Hong-jie, WU Guo-hua, LIU Wen-cai. Microstructure and corrosion behavior of as-homogenized and as-extruded Mg−*x*Li−3Al−2Zn−0.5Y alloys (*x*=4, 8, 12) [J]. Transactions of Nonferrous Metals Society of China, 2022, 32(1): 134−146.

Zn 和 Gd 元素含量和比例对铸态和挤压态 Mg−8Li 合金显微组织和力学性能的影响

黄玉川[1,2,3]，张泉达[1,2]，欧阳思杰[3]，孙福臻[1,2]，
孙家伟[3]，李蕙宇[1,2]，吴国华[3]，陈培军[4]，刘文才[3]

1. 中国机械科学研究总院集团有限公司 先进成形技术与装备国家重点实验室，北京 100083；
2. 北京机科国创轻量化科学研究院有限公司，北京 100083；
3. 上海交通大学 材料科学与工程学院 轻合金精密成型国家工程中心和金属基复合材料重点实验室，上海 200240；
4. 洛阳晟雅镁合金科技有限公司，洛阳 471921

摘　要：研究 Zn 和 Gd 元素含量及其质量比对铸态和挤压态 Mg−8Li 合金显微组织和力学性能的影响。挤压后，析出相破碎。*β*-Li 中分散着粒径约 100 nm 的球形微粒。形成了由长条状 *α*-Mg 粗晶和再结晶 *β*-Li 细晶组成的双峰结构。挤压后合金的强度和塑性显著提高，且屈服强度和极限抗拉强度随 Zn 和 Gd 含量的增加而增加。Mg−8Li−8Zn−2Gd 合金表现出最优的综合性能，其屈服强度、极限抗拉强度和伸长率分别为 274 MPa、283 MPa 和 39.9%。挤压态合金主要强化机制为由 *β*-Li 的细晶强化和 *α*-Mg 的织构强化组成的双模态结构强化和析出相的弥散强化。

关键词：镁锂合金；挤压变形；双峰结构；弥散强化

(Edited by Wei-ping CHEN)